Journal of Machine Engineering, 2022, Vol. 22, No. 3, 148–160
ISSN 1895-7595 (Print) ISSN 2391-8071 (Online)

Received: *03 May 2022* / Accepted: *09 June 2022* / Published online: *13 June 2022*

steam turbine, diaphragm, blade throat, manufacturing processes, geometric deviation, 3D optical scanning

Petr ERET[1*]
Michal HOZNEDL[2]

EFFECT OF MANUFACTURING PROCESSES ON BLADE THROAT SIZE AND POSITION IN A STEAM TURBINE DIAPHRAGM

Despite a sustainable energy future, steam turbines are requisite for the reliability and security of the electric power supply in many countries. Accurate and precise manufacturing of the steam path is crucial to turbine efficiency. Before entering the rotor blades, the steam must be correctly guided using stationary blading in a diaphragm. Steam turbine diaphragms are complicated components to manufacture, and welding is the most common fabrication method. A case study presented in this paper employs data from a 3D optical scanner for a geometric deviation analysis of the upper half of the diaphragm at two production steps, after complete welding and after final machining. Unrolled cylinder cross-sections at different diameters are used to evaluate the blade throat sizes and positions compared to the nominal geometry. The results indicate significant geometric changes between the two fabrication steps, and several suggestions are put forward for targeted future work.

1. INTRODUCTION

Electricity demand is set to increase further [1], and only nuclear power plants can sustainably and reliably supply the large amount of clean and economical energy needed to run industrial companies with minimal greenhouse gas emissions [2]. The share of coal in the global power generation mix continues to decay. Significant initiatives toward the decarbonisation of energy systems have been already undertaken worldwide, and some countries have announced an exit from coal-fired power generation. Investments in carbon-intensive energy infrastructure can be exposed to carbon pricing risk; eventually, some may even become stranded assets [3]. Covid-19 has catalysed a structural fall in global coal need, and even the projected increases in coal demand in developing economies are markedly lower [4]. Renewable energy sources are rising [5], and fossil-fired steam power plants have become the linking element to the renewable energy future. Market perspective and political factors show that for some more decades, coal-fired power plants are predicted to remain a significant

[1] Dept. of Power System Engineering, Faculty of Mechanical Engineering, University of West Bohemia, Czech Republic
[2] Experimental Research of Flow, Doosan Skoda Power, Czech Republic
[*] E-mail: petreret@kke.zcu.cz
https://doi.org/10.36897/jme/150830

contributor to the future power supply mix in various countries to meet the energy demand [6–10]. In synergy with the wind and solar energy sources, coal-fired steam power plants must operate flexibly based on market demand [11–17] and supply electric power with the highest efficiency and the lowest emissions possible. One feasible way to meet the high-efficiency requirements is an optimised turbine steam path with minimal aerodynamic and leakage losses in rotating and stationary components. Accurate and precise manufacturing of the steam path is crucial to turbine efficiency, and geometric deviations caused by production or assembly errors are undesirable. The diaphragm is one of the most crucial parts of the turbine as it redirects the accelerating steam in the correct direction to enter the next row of moving blades. Therefore, diaphragm manufacturing processes must retain the optimum shapes of steam passages.

Welding is the most common, reliable, and cost-effective method of diaphragm fabrication [18], especially in low-pressure turbine stages. A typical welded diaphragm assembly has three main parts: an inner ring, a guide vane row and an outer ring [19]. The guide vane row consists of two concentric slotted rings with stationary blades. The blades are inserted into the slotted rings during the cascade assembly and connected at both ends by technological welds. Subsequently, the guide vane row is assembled with the inner and outer rings and welded together by main welds. The height of such welds must be bounded to avoid an excess deformation of welded structures [20]. After welding is complete, each diaphragm must be stress-relieved and final machined [18]. Thus, the absolute accuracy of the final product geometry cannot be guaranteed, and numerous check and inspection points are included in the diaphragm manufacturing process.

Large temperature gradients, deformations and residual stresses produced in welding turbine components with complex geometries must be investigated as they reduce the service life of components. Berglund et al. [21] simulated the welding and heat treatment of a part of the turbine exhaust case of an aero-engine component. Bendeich et al. [22] measured the residual stress in low-pressure turbine blades repaired by laser cladding. Bonakdar et al. [23] applied finite element modelling to predict the stresses and distortions generated during and after electron beam welding of gas turbine blades. García-García et al. [24] conducted the fluid-structure interaction modelling of expansion-contraction deformation during welding in a spacer-band-blade assembly of high pressure (HP) steam turbine diaphragm. Tan et al. [25] investigated the effect of welding residual stress on operating stress in designing a nuclear turbine welded rotor. Alcantar-Mondragón et al. [26] determined the optimal post-weld heat treatment parameters for 12Cr-1Mo steel, commonly used to manufacture HP steam turbine diaphragms. Emonts et al. [27] studied the thermoelastic deformation of a large scale turbine housing.

Manufacturing processes in diaphragm fabrication also profoundly affect the most critical parameter in turbine blade rows - the throat area, which directly defines the steam mass flow rate through the turbine stages. However, issues with actual throat size and position in the blade channel have received little attention in the literature. For example, Chen et al. [28] inspected assembly accuracy for turbine blades and presented two specifications of assembly error, which are key factors influencing the throat and the incidence of a turbine cascade. The authors showed only the distribution and variation of both errors for rotor blades, and no direct quantification of the throat size had been demonstrated.

A case study presented in this paper quantifies the effect of manufacturing processes on the blade throat size and position in a steam turbine diaphragm comprehensively for the first time. Output datasets from a 3D optical scanner are utilised for geometric variability analysis of an upper half of the nozzle diaphragm at two production steps, after welding and final machining. Unrolled cylinder cross-sections at three different diameters are used to evaluate the blade throat sizes and positions compared to the nominal geometry. The diameters are considered along the leading edge of the diaphragm blade: the first diameter is near the blade root - just above the weld, the second diameter is at the blade mid-span, and the third diameter is near the blade tip. The objective of this study is not to enrich the content of the manufacturing processes of steam turbine diaphragms but put forward targeted future work.

2. STEAM TURBINE DIAPHRAGM GEOMETRIES AND ANALYSIS TOOLS

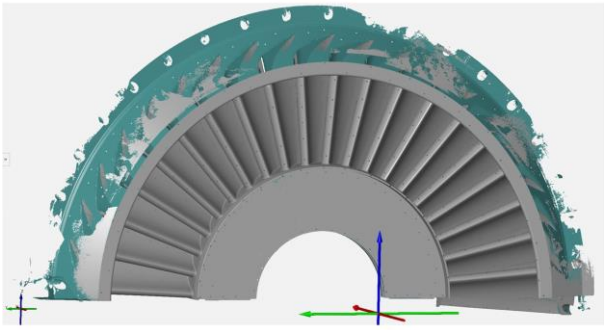

Fig. 1. Actual geometry of upper half of nozzle diaphragm, after complete machining

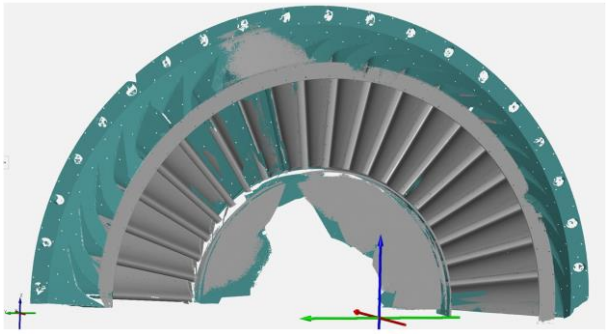

Fig. 2. Actual geometry of upper half of nozzle diaphragm, after complete welding

The upper half of a steam turbine diaphragm consisting of 20 last stage blades was examined in this work. The hub radius is about 810 mm, and the length of the stator blade is 530 mm at the leading edge and 770 mm at the trailing edge. Fig. 1 depicts the actual geometry of the assembly after complete machining with all blades scanned. Unfortunately, a part of the geometry was not digitalised after complete welding due to the limited time available for inspecting the diaphragm. The actual geometry scanned after welding is shown in Fig. 2. Thus, several incompletely scanned blades have been omitted from the analysis; five profiles at the blade root and four at the blade mid-span and the blade tip. These are specified using a schematic in Fig. 3. Therefore, only 13 blade throats at the root diameter and 14 at the blade mid-span and the blade tip have been considered to compare the two production steps.

A GOM ATOS III Triple Scan + TRITOP digitising system was used to construct exact 3D models. The optical scanner is frequently employed in research studies as it guarantees high data quality with minimum noise [29, 30]. It is based on advanced projection technology of structured blue light and has two 8 megapixel cameras, and this high-performance device can provide a typical point spacing of 0.01 mm. The system can control the influence of environmental conditions and automatically transforms all measurements into a common object coordinate system. Datasets are then easily exported using standard file formats for

post-processing. The associated GOM Inspect software executes the best fit alignment between the actual mesh and the model geometry and constructs the unrolled cylinder cross-sections. Figure 4 depicts the surface deviation map between the actual and model geometry of the diaphragm after machining. The map uses the RGB colour model with green as the zero deviation, red as the positive maximum deviation and blue as the negative maximum deviation (the colour range is confidential).

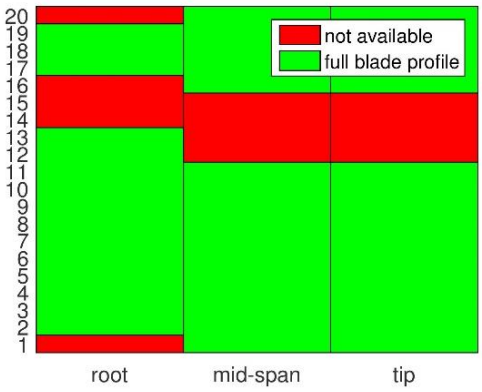

Fig. 3. Schematic of fully scanned diaphragm blades after welding

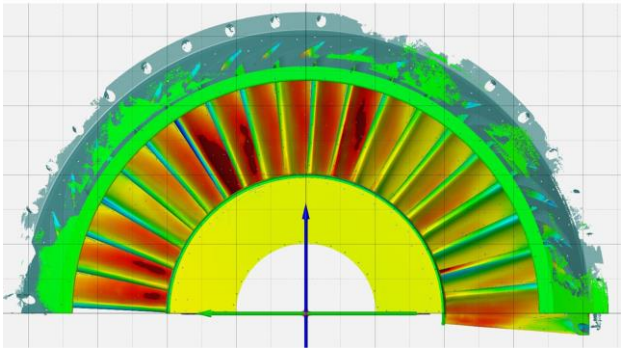

Fig. 4. Surface deviation map between the actual and model geometry of diaphragm after machining, downstream view (colour online)

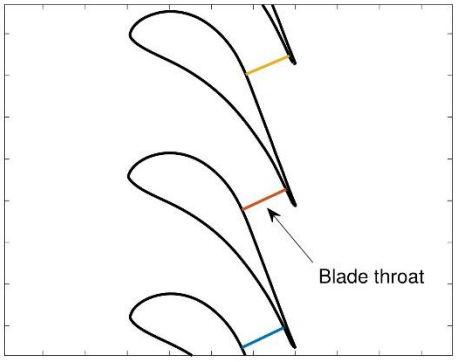

Fig. 5. Unrolled cylinder cross-section of diaphragm blade profiles at the blade mid-span with identified throats, after machining

The unrolled cylinder cross-section data were further processed in Matlab to estimate the geometric variability of blade throat sizes and positions. First, throats are determined using a minimal distance search algorithm between the adjacent blade curves. Figure 5 depicts the unrolled cylinder cross-section of blade profiles after machining at the blade mid-span with identified throats. The geometry of thoroughly scanned blades is analysed (i.e. after machining) at first, histograms are used to display the blade throat sizes normalised by nominal values, and relative variations are presented in percentages with nominal values set to zero. The optimal numbers of bins in histograms have been calculated using a technique proposed by Shimazaki and Shinomoto [31]. A comparison between the production steps is performed afterwards on selected blade throats using correlation estimations. In addition, blade throat position changes after each manufacturing step are presented in a vector plot, and the data are shown in a non-dimensional form, divided by the nominal blade throat size.

Pearson correlation coefficient R, which defines the strength of a linear relationship between two variables and their association with each other, is also used in the analysis further. Eq. 1 shows the expression for R,

$$R = \frac{\sum_{i=1}^{n}(x_i - \bar{x})(y_i - \bar{y})}{\sqrt{\sum_{i=1}^{n}(x_i - \bar{x})^2 \sum_{i=1}^{n}(y_i - \bar{y})^2}} \tag{1}$$

where n is the sample size, x_i and y_i are the individual sample points indexed with i and $\bar{x}$ represents the sample mean (analogously for $\bar{y}$).

The parameter R yields a value of +1 (total positive linear correlation), when every positive increase in one variable corresponds to a positive increase of a fixed proportion in the other. The correlation coefficient R is equal to –1 for the case of total negative linear correlation and zero for no linear correlation. The strength of linear relationship between two variables is generally considered strong for $|R| > 0.7$, moderate for $0.7 > |R| > 0.5$, weak for $0.5 > |R| > 0.3$ and none or very weak for $|R| < 0.3$.

3. RESULTS

3.1. DIAPHRAGM AFTER MACHINING

Figures 6 to 8 depict the distributions of diaphragm blade throat values after complete machining for all twenty scanned blades at different diameters. Although the histograms are based on relatively little data, the technique proposed by Shimazaki and Shinomoto [31] produces meaningful histogram patterns. The histogram patterns are unimodal and non-symmetric at all diameters. The error between the mean and nominal value is 1% at the blade root. In addition, a negative error of –1.45% can be observed at the blade mid-span, and a positive error of 0.63% is at the blade tip. Positions of the histograms to the nominal values suggest that the manufacturing of diaphragm blades is reasonably accurate but imprecise. For example, the relative error in Fig. 7 at the blade mid-span ranges from –5% to +2% approximately.

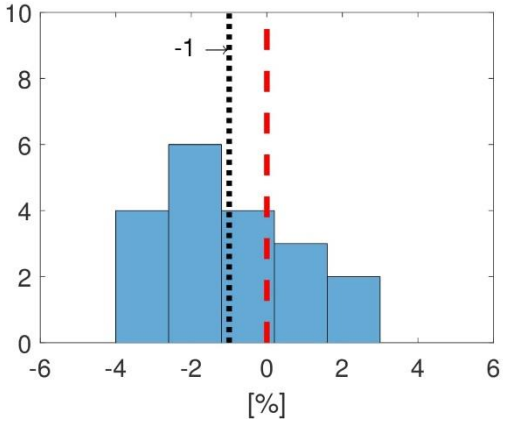

Fig. 6. Histogram of the diaphragm throat after machining at the blade root: mean (⋯) and nominal (- - -)

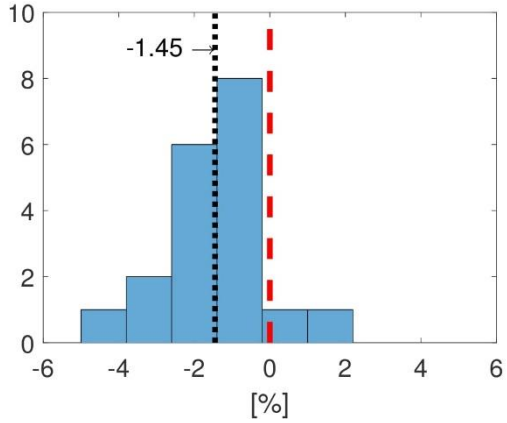

Fig. 7. Histogram of the diaphragm throat after machining at the blade mid-span: mean (⋯) and nominal (- - -)

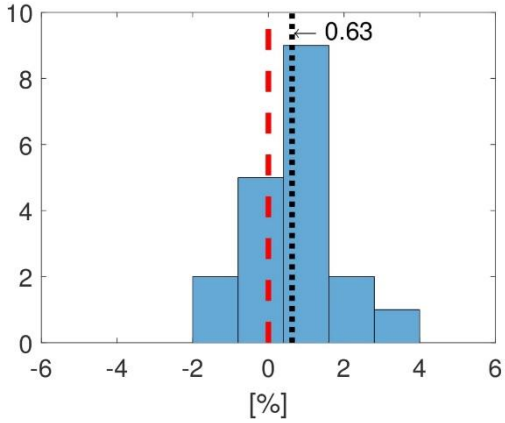

Fig. 8. Histogram of the diaphragm throat after machining at the blade tip: mean (⋯) and nominal (- - -)

Figure 9 shows the data for a relation between the throat size at the blade mid-span and the blade tip. It is expected that an increase in throat size at the blade mid-span will strongly correlate with an increase in the throat size at the blade tip. The scatter plot includes linear regression, and the analysis is completed by estimating the Pearson correlation coefficient *R*. It was found that the throat sizes at the blade mid-span and the blade tip have a nearly total positive correlation $R = 0.94$. Figure 10 depicts the scatter plot of a relation between the throat size at the blade root and the throat size at the blade mid-span. Outliers have an enormous impact on the conventional measure of correlation and reduce the value of *R*, see example in [32]. The analysis revealed a positive correlation $R = 0.75$ for the throat size at the blade root and the blade mid-span. Manufacturing errors cause the reduction of the correlation strength due to the deformations in the circumference weld around the blade root. The welding influence on the blade throat size is fully captured in the associated unrolled cylinder cross-section. In contrast, unrolled cylinder cross-section at the blade tip can describe the welding effect only at the leading edge, as the blade length increases towards the trailing edge, and no influence of the welding on the blade throat size is observed.

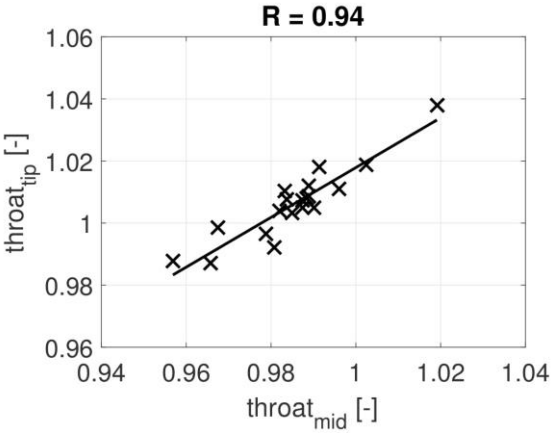

Fig. 9. Correlation of the throat size after machining: mid-span/tip

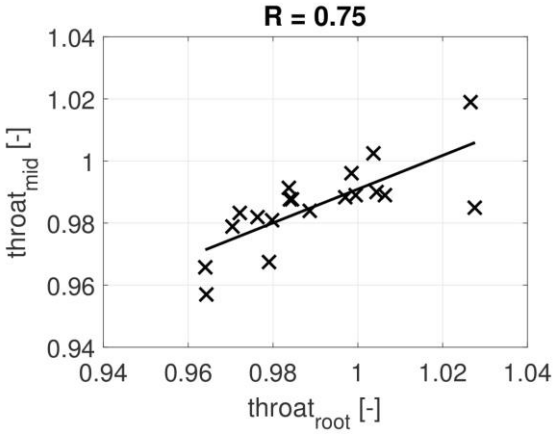

Fig. 10. Correlation of the throat size after machining: root/mid-span

Figure 11 compares the actual and nominal unrolled cylinder cross-sections with blade profiles and throats at the blade mid-span after machining. The plot clearly illustrates the upstream shifts of some blade throat positions, resulting in a non-uniform distribution of steam flow as the converging blade channels with a steady acceleration of the flow up to the throat change into the converging-diverging blade channels. Figures 12 to 14 depict the vector plots of blade throat centre shifts after machining at different diameters. The data are shown in a non-dimensional form, divided by the nominal blade throat size (th_{nom}). No throat can be found in the design position, and most of the blade throats are shifted upstream of the nominal blade throat position. Table 1 summarises the upstream and downstream blade throat centre shifts. The magnitudes of upstream blade throat dislocations are major; in one case, the distance is over 30% of the nominal blade throat size. Figure 15 shows the relative magnitude of the blade throat shift d/th_{nom} at the blade mid-span, and blade throat #7 has a value of 34%. In addition, the dissimilarities in the blade throat positions might negatively affect the essential function of diaphragm blading. Therefore, further study using CFD is recommended.

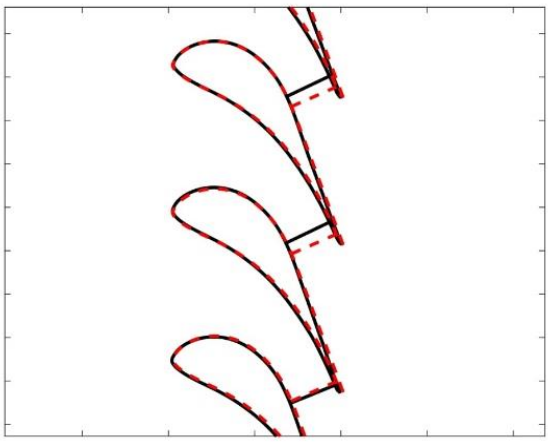

Fig. 11. Actual and nominal unrolled cylinder cross-sections with blade profiles and throats at the blade mid-span after machining: actual (-) and nominal (- - -)

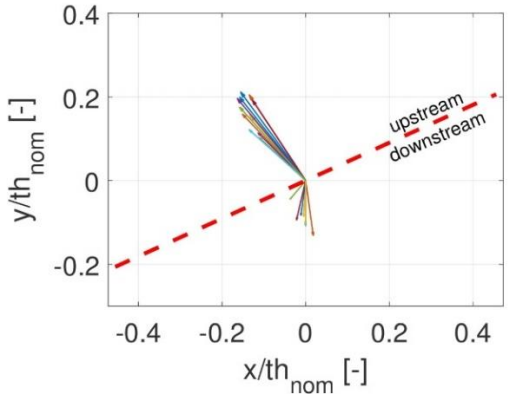

Fig.12. Blade throat centre shift after machining at the blade root: (- - -) position of nominal throat

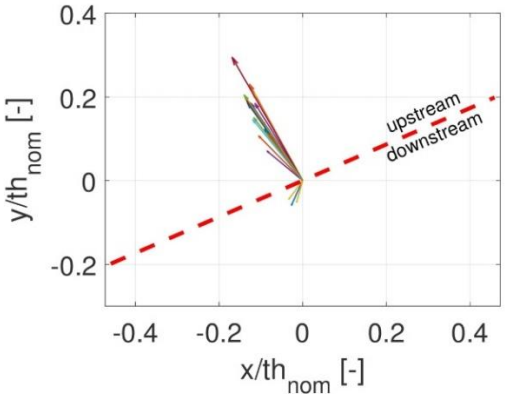

Fig.13. Blade throat centre shift after machining at the blade mid-span: (- - -) position of nominal throat

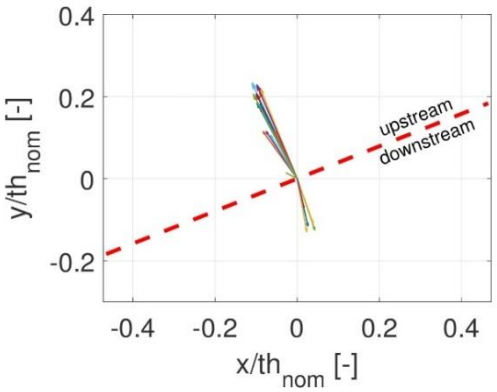

Fig. 14. Blade throat centre shift after machining at the blade tip: (- - -) position of nominal throat

Table 1. Count of blade throat centre shifts after machining

Blade diameter	Upstream	Downstream
root	12	7
mid-span	16	3
tip	14	5

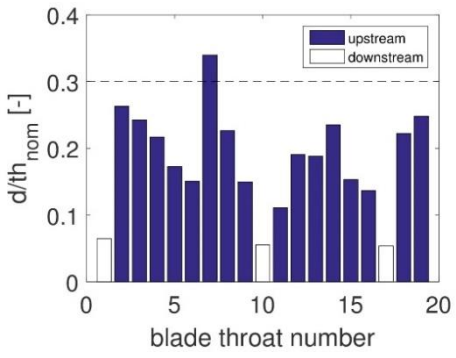

Fig. 15. Bar plot of the relative magnitude of blade throat shift after machining at the blade mid-span, respecting upstream or downstream position

3.2. COMPARISON BETWEEN THE PRODUCTION STEPS

As explained previously, the production steps were compared using 13 blade throats at the root diameter and 14 blade throats at the blade mid-span and the blade tip. The analysis outputs are summarised in Fig. 16, where the line plots of blade throat mean values at three different diameters for both manufacturing processes are depicted. A scatter in the data is demonstrated using the vertical error bars based on standard deviations. A drop in the data suggests that the machining has systematically affected the blade throat size at all diameters. The overall discrepancy between the actual and nominal geometry has deteriorated. The mean value of the relative error for the three diameters is 0.43% after welding and −0.61% after machining. Figure 17 shows the data for a relation between the throat size after welding and the blade throat size after machining at the different diameters. None or very weak relationships can be seen in the scattered data, and this is confirmed by the evaluation of the correlation coefficient, which yields R = 0.31 at the blade root, R = −0.13 at the blade mid-span, and R = 0.16 at the blade tip, respectively. Therefore, each manufacturing step has a different impact on the diaphragm geometry. This finding confirms the need to perform numerous inspections in each step of the diaphragm manufacturing process.

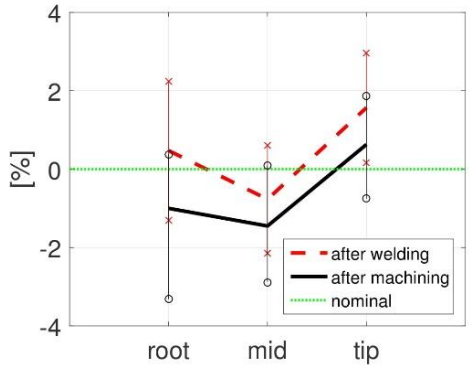

Fig. 16. Line plots of blade throat mean values with error bars

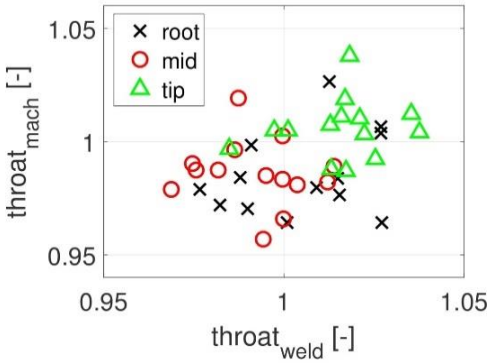

Fig. 17. Correlation of the throat size after welding and after machining

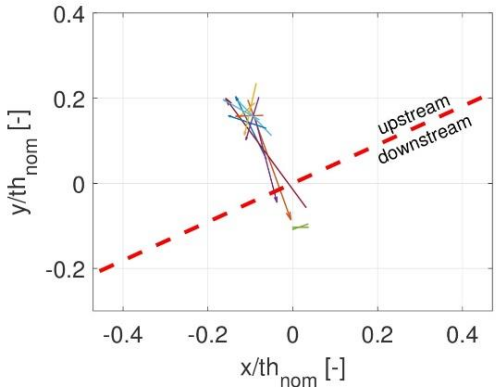

Fig. 18. Vector plot of blade throat centre position change between the production steps at the blade root: (- - -) position of nominal throat

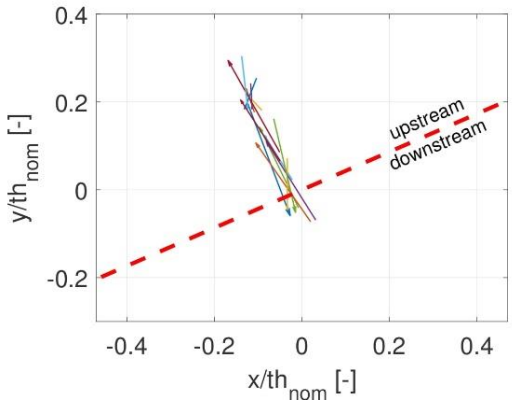

Fig. 19. Vector plot of blade throat centre position change between the production steps at the blade mid-span: (- - -) position of nominal throat

The analysis showed that, between the two manufacturing processes, several actual blade throats have entirely switched positions from an upstream to a downstream location (with respect to the nominal blade throat position) and vice versa. There are three such blade throats at the blade root, six at the blade mid-span, and five at the blade tip, as shown using the vector plots in Figs 18 to 20. They can be associated with the magnitude of the relative blade throat centre shift $d/th_{nom} \geq 20\%$, as depicted in Figures 21 to 23. The switchover can be best manifested using blade throat #1 at the tip diameter, where the downstream blade throat centre shift is nearly 40% of the nominal blade throat size. Other significant blade throat dislocations ($\geq 30\%$) can be observed on blade throats #2 & #7 at the blade root and #12 & #13 at the blade tip. After each manufacturing step, only a few blade throats are approximately at the same positions. Blade throats #2 & #5 at the tip diameter have a minor position change, and the relative magnitude of the blade throat centre is up to 2% of the nominal blade throat size. Blade throats #5 & #12 at the blade root diameter, #3 at the blade mid-span and #10 at the blade tip have the relative magnitude of blade throat centre shift up to 5% of the nominal blade throat size. Thus, the overall view of Figs 21 to 23 shows that machining has irregularly affected the blade throats. This finding, together with the previous results, suggests applying more measures for the higher accuracy of blade geometry in technological processes of diaphragm manufacturing.

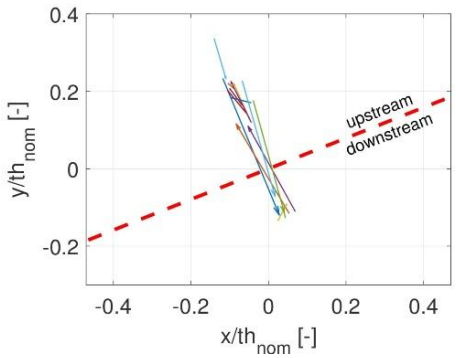

Fig. 20. Vector plot of blade throat centre position change between the production steps at the blade tip: (- - -) position of nominal throat

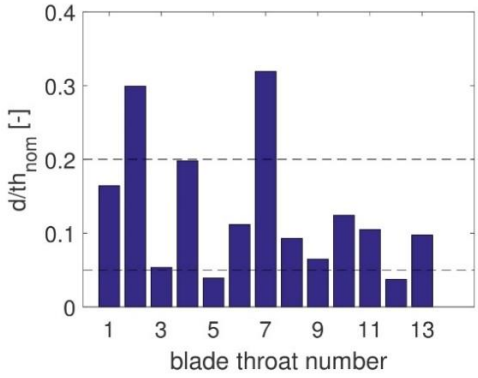

Fig. 21. Bar plot of the relative magnitude of blade throat centre shift between the production steps at the blade root, not respecting upstream or downstream position

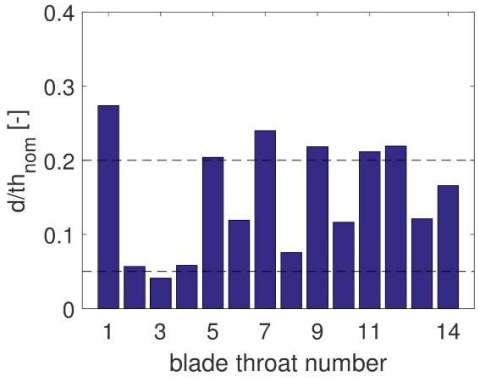

Fig. 22. Bar plot of the relative magnitude of blade throat centre shift between the production steps at the blade mid-span, not respecting upstream or downstream position

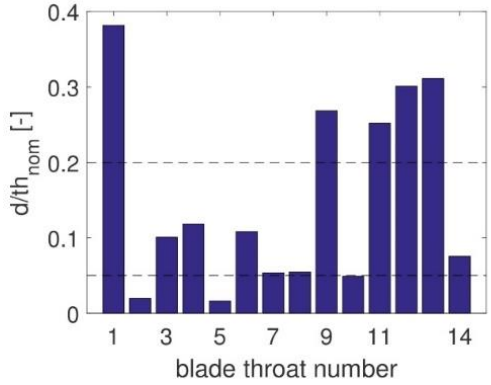

Fig. 23. Bar plot of the relative magnitude of blade throat centre shift between the production steps at the blade tip, not respecting upstream or downstream position

4. CONCLUSION

The effect of two manufacturing processes on the blade throat size and position in a steam turbine diaphragm has been investigated. Digitalised geometries of the upper half of the nozzle diaphragm after complete welding and after machining were used to evaluate the blade throat sizes and positions using unrolled cylinder cross-sections at three different diameters - near blade root, mid-span and blade tip and compared to the nominal geometry. The geometric errors of blade throat size were estimated, and different mean values were observed for welding and machining. The obtained data seem reasonably accurate but not precise, and the mean values suggested that the machining has systematically and negatively affected the overall agreement between the actual and nominal geometry. None or very weak relationships in the blade throat size have been observed between the two manufacturing steps. The analysis also pointed out the dislocations of actual blade throats to the nominal blade throat position. The vast majority of the blade throats were shifted upstream of the nominal blade throat, and the magnitudes of these dislocations were large. In one case, the distance was over 30% of the nominal blade throat size. These dissimilarities in the blade throat positions might negatively affect the essential function of diaphragm blading, and a further CFD study was recommended. Moreover, after machining, some actual blade throats have completely switched position from an upstream to a downstream location to the nominal blade position and vice versa, and it was shown that the machining process had affected the blade throats irregularly. The results indicated significant geometric changes between the two fabrication steps, and it was suggested to apply more measures for the higher accuracy of blade geometry in technological processes of diaphragm manufacturing.

ACKNOWLEDGEMENTS

This study was financially supported by the Ministry of Education, Youth and Sports of the Czech Republic under grant agreement No. CZ.02.1.01/0.0/0.0/16 026/0008389. The authors also thank Doosan Skoda Power for the permission to publish this paper and the 3D Scanning and Reverse Engineering Team of Doosan Skoda Power for providing the data.

REFERENCES

[1] KOBER T., SCHIFFER H.W, DENSING M., et al., *2019, Global Energy Perspectives to 2060 – WEC's World Energy Scenarios*, Energy Strategy Reviews, 2020, 31, 100523.

[2] BROOK B.W., ALONSO A., MENELEY D.A., et al., 2014, *Why Nuclear Energy is Sustainable and Has to be Part of the Energy Mix*, Sustainable Materials and Technologies, 1/2, 8–16.

[3] MO J., CUI L., DUAN H., 2021, *Quantifying the Implied Risk for Newly-Built Coal Plant to Become Stranded Asset by Carbon Pricing*, Energy Economic, 99, 105286.

[4] IEA., World Energy Outlook 2020, URL https://www.iea.org/reports/world-energy-outlook-2020.

[5] GIELEN D., BOSHELL F., SAYGIN D., et al., 2019, *The Role of Renewable Energy in the Global Energy Transformation*, Energy Strategy Reviews, 24, 38–50.

[6] FUNAHASHI N., 2017, *22 – Steam Turbine Roles and Necessary Technologies for Stabilization of the Electricity Grid in the Renewable Energy Era*, Tanuma T (ed.) Advances in Steam Turbines for Modern Power Plants, Woodhead Publishing,. 521–537, ISBN 978-0-08-100314-5.

[7] TOPEL M., LAUMERT B., 2018, *Improving Concentrating Solar Power Plant Performance by Increasing Steam Turbine Flexibility at Start-Up*, Solar Energy, 165, 10–18.

[8] FROEHLICH J., 2019, *Full Steam Ahead*, World Coal, 28/4, 31–34.

[9] NAWAZ Z., ALI U., 2020, *Techno-Economic Evaluation of Different Operating Scenarios for Indigenous and Imported Coal Blends and Biomass Co-Firing on Supercritical Coal Fired Power Plant Performance*, Energy, 212, 118721.

[10] CLARK R., ZUCKER N., URPELAINEN J., 2020, *The Future of Coalfired Power Generation in Southeast Asia*, Renewable and Sustainable Energy Reviews, 121, 109650.

[11] ZHAO Y., WANG C., LIU M., et al. 2018, *Improving Operational Flexibility by Regulating Extraction Steam of High-Pressure Heaters on a 660 MW Supercritical Coal-Fired Power Plant: A Dynamic Simulation*, Applied Energy, 212, 1295–1309.

[12] RICHTER M., OELJEKLAUS G., GORNER K., 2019, *Improving the Load Flexibility of Coal-Fired Power Plants by the Integration of a Thermal Energy Storage*, Applied Energy, 236, 607–621.

[13] STEVANOVIC V.D., PETROVIC M.M, MILIVOJEVIC S., et al., 2020, *Upgrade of the Thermal Power Plant Flexibility by the Steam Accumulator*, Energy Conversion and Management, 223, 113271.

[14] NOWAK G., RUSIN A., ŁUKOWICZ H., et al., 2020, *Improving the Power Unit Operation Flexibility by the Turbine Startup Optimization*. Energy, 198, 117303.

[15] YAN H., LI X., LIU M., et al., 2020, *Performance Analysis of a Solar-Aided Coal-Fired Power Plant in off-Design Working Conditions and Dynamic Process*, Energy Conversion and Management, 220, 113059.

[16] WANG Z., LIU M., ZHAO Y., et al., 2020, *Flexibility and Efficiency Enhancement for Double-Reheat Coal-Fired Power Plants by Control Optimization Considering Boiler Heat Storage*, Energy, 201, 117594.

[17] RUSIN A., NOWAK G., ŁUKOWICZ H., et al., 2021, *Selecting Optimal Conditions for the Turbine Warm and Hot Start-Up*, Energy, 214, 118836.

[18] GOLINKIN S., LIPSKI M., LUKER J., et al., 2013, *Modernization of Steam Turbine Diaphragms for the Saudi Aramco Gas Plant*, Proceedings of Middle Eastern Turbomachinery Symposium, 7–20 March, Doha, Qatar.

[19] MCBEAN I., 2017, *16 - Manufacturing Technologies for Key Steam Turbine Parts*, Tanuma T. (ed.) Advances in Steam Turbines for Modern Power Plants, Woodhead Publishing, 381–393, ISBN 978-0-08-100314-5.

[20] TSARYUK A., SKULSKY V., NIMKO M., et al., 2016, *Improvement of the Technology of Welding High-Temperature Diaphragms in Steam Turbine Flow Section*, The Paton Welding Journal, 3, 24–27.

[21] BERGLUND D., ALBERG H., RUNNEMALM H., 2003, *Simulation of Welding and Stress Relief Heat Treatment of an Aero Engine Component*, Finite Elements in Analysis and Design, 39/9, 865–881.

[22] BENDEICH P., ALAM N., BRANDT M., et al., 2006, *Residual Stress Measurements in Laser Clad Repaired Low Pressure Turbine Blades for the Power Industry*, Materials Science and Engineering, A 437/1, 70–74.

[23] BONAKDAR A., MOLAVI-ZARANDI M., CHAMANFAR A., et al., 2017, *Finite Element Modeling of the Electron Beam Welding of Inconel-713LC Gas Turbine Blades*, Journal of Manufacturing Processes, 26, 339–354.

[24] GARCIA-GARCIA V., CAMACHO-ARRIAGA J., REYES-CALDERON F., et al., 2018, *Fluid Structure Interaction Modeling of Expansion Contraction Deformation During Welding in a Spacer-Band-Blade Assembly of a HP Steam Turbine Diaphragm*, Journal of Manufacturing Processes, 33, 203–218.

[25] TAN L., ZHAO L., ZHAO P., et al., 2020, *Effect of Welding Residual Stress on Operating Stress of Nuclear Turbine Low Pressure Rotor*, Nuclear Engineering and Technology, 5/8, 1862–1870.

[26] ALCANTAR-MONDRAGON N., REYES-CALDERON F., GARCIA-GARCIA V., et al., 2021, *Effect of PWHT on the Dissolution of δ-Ferrite in the Welded Joint of 12Cr–1Mo Steels for Steam Turbines*, Journal of Materials Research and Technology, 10, 1262–1279.

[27] EMONTS D., SANDERS M.P., MONTAVON B., SCHMITT R.H., 2022, *Model-Based, Experimental Thermoelastic Analysis of a Large Scale Turbine Housing*, Journal of Machine Engineering, 22/1, 84–95.
[28] CHEN L., LI B., JIANG Z., 2017, *Inspection of Assembly Error with Effect on Throat and Incidence for turbine Blades*, Journal of Manufacturing Systems, 43, 366–374.
[29] GAO J., GINDY N., CHEN X., 2006, *An Automated GD&T Inspection System Based on Non-Contact 3D Digitization*, International Journal of Production Research, 44/1, 117–134.
[30] BAUER F., SCHRAPP M., SZIJARTO J., 2019, *Accuracy Analysis of a Piece-to-Piece Reverse Engineering Workflow for a Turbine Foil Based on Multi-Modal Computed Tomography and Additive Manufacturing*, Precision Engineering, 60, 63–75.
[31] SHIMAZAKI H., SHINOMOTO S., 2007, *A Method for Selecting the Bin Size of a Time Histogram*, Neural Computation, 19/6, 1503–1527.
[32] KIM Y., KIM T.H., ERGUN T., 2015, *The Instability of the Pearson Correlation Coefficient in the Presence of Coincidental Outliers*, Finance Research Letters, 13, 243–257.